Electrical Modulation of the Local Conduction at Oxide Tubular Interfaces

Ying-Hui Hsieh,[†,⊥] Evgheni Strelcov,[‡,⊥] Jia-Ming Liou,[§] Chia-Ying Shen,[†] Yi-Chun Chen,[§] Sergei V. Kalinin,[‡] and Ying-Hao Chu[†,*]

[†]Department of Materials Science and Engineering, National Chiao Tung University, Hsinchu 30010, Taiwan, [‡]Center for Nanophase Materials Sciences, Oak Ridge National Laboratory, Oak Ridge, Tennessee 37831, United States, and [§]Department of Physics, National Cheng Kung University, Tainan 70101, Taiwan. [⊥]Y.-H. Hsieh and E. Strelcov contributed equally.

ABSTRACT Heterointerfaces between complex oxides have sparked considerable interest due to their fascinating physical properties and their offering of new possibilities for next-generation electronic devices. The key to realize practical applications is the control through external stimuli. In this study, we take the self-assembled $BiFeO_3$—$CoFe_2O_4$ tubular interface as a model system to demonstrate the nonvolatile electric control of the local conduction at the complex oxide tubular interface. The fundamental mechanism behind this modulation was explored based on static and dynamic conductive atomic force microscopies. We found the movement of oxygen vacancies in the $BiFeO_3$—$CoFe_2O_4$ heterostructure is the key to drive this intriguing behavior. This study delivers a possibility in developing next-generation electronic devices.

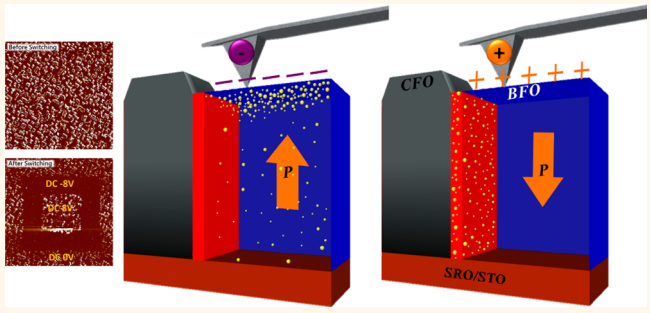

KEYWORDS: tubular interface · BFO—CFO · oxygen vacancy · conductive AFM · FORC-IV

Complex oxide interfaces are emerging as one of the most exciting subjects in the field of condensed matter due to their unique physical properties and their possibilities for next-generation electronic devices.[1,2] Three types of complex oxide interface have been established.[3] Among them, the most explored interface is the artificially constructed heterointerface. Various interactions at the interface have resulted in a number of exciting discoveries, such as the formation of a highly mobile quasi-two-dimensional electron gas (2DEG) between two insulators ($LaAlO_3$ and $SrTiO_3$).[4] Moreover, in ferroic oxides, domain walls dictate natural homointerfaces as a consequence of the minimization of electrostatic and elastic energies.[5] Several key studies have pointed out the interesting observation of the existence of local conduction on domain walls in ferro/multiferroics.[6−9] Recently, a new tubular oxide interface has been developed in the self-assembled heterostructures, and local conduction at the tubular interfaces of the $BiFeO_3$ (BFO)—$CoFe_2O_4$ (CFO) heterostructure was discovered.[3] Such results create a huge playground to explore and design intriguing properties of complex oxide interfaces. However, in the push for practical applications, control of the interface functionalities through external stimuli is desirable. An electrical modulation of the local conduction at the homo- (BFO domain walls) and heterointerfaces ($LaAlO_3$/$SrTiO_3$) was demonstrated recently.[10,11] In this study, we showed that the BFO—CFO tubular interface conduction could be modulated nonvolatilely and reversibly *via* an external electric field. A memristive-like electronic conduction was observed, which is strongly correlated to the motion of oxygen vacancies (donor impurities) at the interface and in turn modified the characteristics of the junction between the measurement tip and the interface. Our results complete the control of the conduction at complex oxide interfaces and suggest the possibility for new devices based on complex oxide interfaces.

RESULTS AND DISCUSSION

BFO—CFO nanocomposite films of 100 nm were grown on 30 nm $SrRuO_3$ (SRO)-buffered STO (001) substrates by pulsed laser deposition assisted by high-pressure reflective high-energy electron diffraction to *in situ* monitor the growth process.[12] Figure 1(a) shows an illustration of the BFO—CFO

* Address correspondence to yhc@nctu.edu.tw.

Received for review June 1, 2013 and accepted September 9, 2013.

Published online September 09, 2013
10.1021/nn402763w

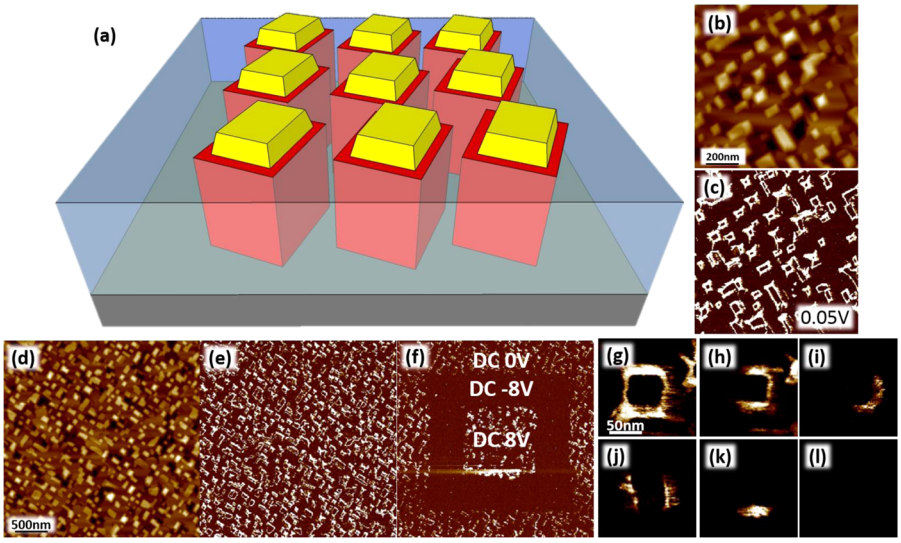

Figure 1. (a) Diagram of BFO−CFO nanostructures. CFO nanopillars (yellow) are embedded in the BFO matrix (blue), and hence tubular interfaces (red) form between these two materials. (b) Topography and (c) current image of BCFO are gained simultaneously under the C-AFM mode, where the current is read by applied −0.05 V tip bias. (d−f) Conduction currents at tubular interfaces can be turned on and off by applying a larger dc bias (8 V) of different polarity. (g−l) Currents at four sides of the tubular interface can be switched individually.

nanostructures. Due to the surface energy anisotropy, perovskite BFO and spinel CFO phases are spontaneously separated during the heteroepitaxial growth.[13] The CFO nanopillars alternated with the ferroelectric BFO matrix and grew perpendicular to the substrate from bottom to top. The sharp interface between CFO and BFO lies in the {110} orientation, in which the octahedra in the perovskite directly contact those in the spinel phase to lower the interface energy.[14] To investigate the conduction properties of the BFO−CFO composite film, we used SRO as the bottom electrode for electrical characterization and employed conductive atomic force microscopy (C-AFM), an effective technique to probe local conduction with nanoscale spatial resolution,[15] to map current distribution on the sample. The characterization and manipulation of *I*−*V* (current−voltage) behaviors at the interface were also performed by C-AFM. The spatial resolution is limited by the tip radius of 20 nm. Figure 1(b) shows a typical AFM topographic image of BFO−CFO self-assembled nanostructures, where well-orientated CFO pillars are embedded in the BFO matrix. Unlike the matrix and pillar, conducting currents at the interface can be detected under very low tip bias (−0.05 V, Figure 1(c)), which indicates the local conduction behaviors at the tubular interface.

For practical applications, searching for external stimuli to control the local conduction at the interface is the next key step. Reports on oxides, including BFO, have shown that the movement of oxygen vacancies can lead to memristive conducting behaviors.[10,16] In the BFO−CFO system, we also found a similar phenomenon. The variation of local conduction at the tubular interface with a dc bias is directly visualized through the C-AFM. At a small measuring tip bias of −0.5 V, local conduction currents at tubular interfaces are observed in as-grown films (Figure 1(e)). After applying a relatively large dc bias with a magnitude of 8 V on the film by point-to-point tip scanning, the interface shows nonvolatile conduction switching. In Figure 1(f), the larger square was switched by a negative tip bias, and then the smaller square inside the larger one was switched in series by a positive tip bias. The C-AFM image shows that the local conduction diminished in the region poled by a negative tip bias, but it switched back after the region was poled by a positive tip bias. In fact, more precise data analysis indicates that the conduction current can be improved even at the regions poled by a positive bias. More interestingly, the conduction modulation at different sides of the tubular interfaces can be controlled independently. As shown in Figure 1(g−l), each side of the tubular interface was locally switched by the SPM tip. However, the redistribution of the oxygen vacancies can bring up the local conduction again. The relaxation time depends on the applied voltage. This suggests one more pathway to control this local conduction.

To investigate the effect of external bias on the conduction at the tubular interface more quantitatively, we applied pulse voltages on the interface as the modulation source. The magnitude and the duration of the switching bias can thus be controlled. Figure 2 shows the variation of conduction currents at the interface when switching the conduction from OFF to ON state by different pulse voltages. The OFF state was initially created by erasing the local conduction at the interface using a tip bias of −8 V. *I*−*V* curves in Figure 2(a and c) were measured in the range of bias voltage less than 3 V.

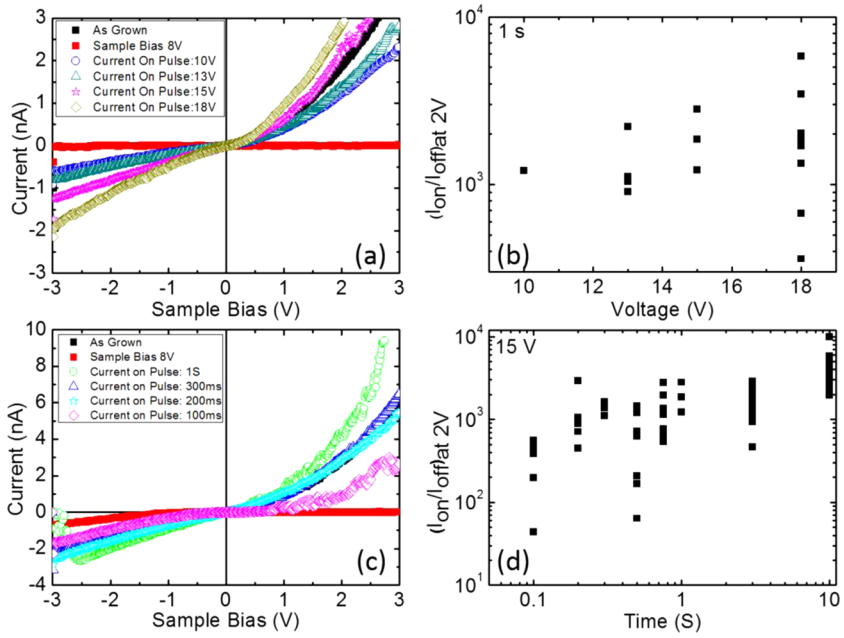

Figure 2. Change of *I*−*V* characteristics at the interface after various external pulse bias was applied. The current (as grown, black dot in (a) and (c)) at the tubular interface was first erased by applying a −8 V tip bias, and then the currents were revived by the voltage pulses. (a) *I*−*V* curves measured after applying negative voltage pulses of different magnitude for 1 s and (b) the conductance ratio of I_{on}/I_{off} measured at 2 V *versus* pulse magnitude. The revived currents increase with the magnitude of voltage pulses. (c) *I*−*V* curves measured after applying −15 V voltage pulses of different duration and (d) the conductance ratio of I_{on}/I_{off} measured at 2 V *versus* pulse duration.

The *I*−*V* curves were tested repeatedly to confirm the measuring bias is small enough to not affect the nonvolatile conduction state. At the interface of the as-grown film (ON state), the *I*−*V* curves can be fitted within the space-charge-limit model, where *I*−*V* plots with the characteristics of $I \propto V^n$ nearly pass through the origin. Figure 2(a) shows that after applying a pulse voltage for 1 s duration, the conduction at the tubular interface was recovered stably if the voltage magnitude is higher than 10 V, and the conductivity at the interface increases with the switching pulse voltages. For switching voltages higher than 15 V, the conduction currents are even higher than those in the as-grown film. The conduction currents of these ON states are on the order of nA. Compared to the currents of the OFF state, which are undetectable in the system limit and estimated to be within the noise level of 10 pA, the conductivity ratio between the ON/OFF state is larger than 10^2. Due to the nonlinear behavior of the *I*−*V* curves, the ratio of I_{on}/I_{off} increases with the detecting bias. Figure 2(b) shows the current ratio measured at 2 V, and the data points are obtained by applying different pulse amplitudes for 1 s duration at various interfaces. The absolute value of obtained ratio fluctuation depends on the tip-to-sample contact condition; on the other hand, the basic trends of increasing ratio with the pulse voltages and large I_{on}/I_{off} ratio of about 10^2 to 10^4 are clear.

The conduction modulation at the interface under different bias durations was also investigated. Figure 2(c) shows that when the pulse magnitude is fixed at 15 V, the conduction at the interface can be reliably recovered once the duration of the voltage pulse is longer than 200 ms, and the nonvolatile conductivity increases with the duration. In contrast, conduction recovery by a duration of less than 100 ms becomes much more difficult, which might require higher applied voltage. Potentially, this can be an obstacle for practical applications. The effect of the duration time on the I_{on}/I_{off} ratio is shown in Figure 2(d), which also illustrates the tendency of increasing ratio with the duration time. The long response time implies the movement of oxygen vacancies as the most possible mechanism for this conduction modulation.

The suggested switching mechanism calls for investigation of oxygen vacancy dynamics and its bias dependence. This was done by using the first-order reversal curve current−voltage (FORC-IV) imaging technique, as it allows probing electrochemical activity locally.[17] A voltage waveform consisting of several triangular pulses with increasing amplitude was applied to the sample *via* an SPM tip, and a current response was recorded. When the measurements were completed at a given location, the tip moves to the next one and the measurements were repeated. Figure 3(a) displays the voltage waveform with three peak biases, 3, 5, and 7 V, and the average current response collected from a spatial grid of 50 × 50 pixels in a region of 500 × 500 nm^2. The corresponding *I*−*V* curves (again, averaged over 2500 pixels with different responses) are shown in Figure 3(b). At peak biases lower than *ca.* 3 V, the *I*−*V* curves are nonhysteretic, with lower and upper branches coinciding (blue line in Figure 3(b)). This

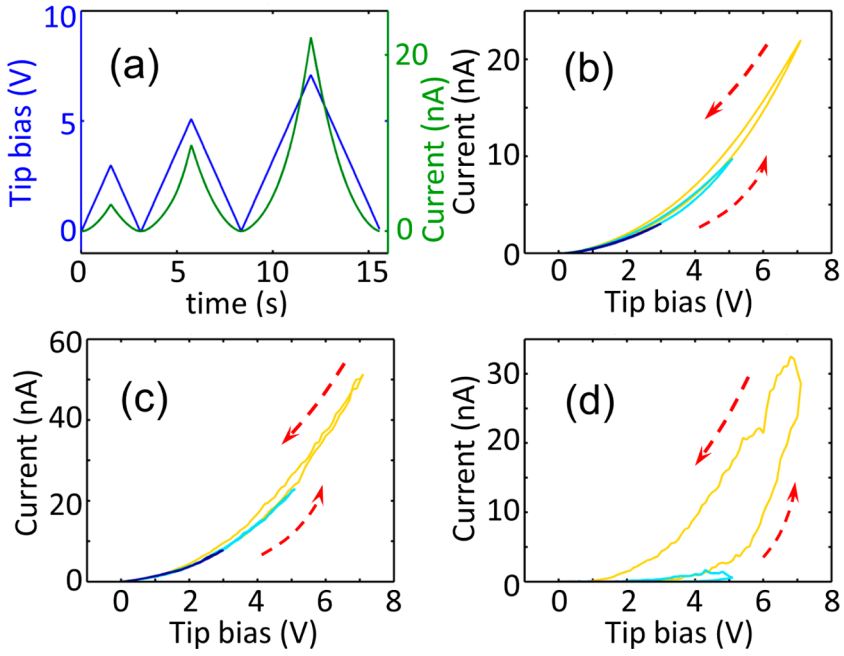

Figure 3. (a) FORC voltage waveform applied to the tip and current response averaged over the 2500 pixels of the grid; (b) corresponding averaged *I*−*V* curves showing some hysteresis; (c) *I*−*V* curves averaged over the top 10% of pixels with highest conductivity showing little hysteresis; (d) *I*−*V* curves averaged over the top 10% of pixels with highest loop area showing significant hysteresis but lower conductivity.

means that the bias sweep to lower peak values does not shift oxygen vacancies around and thereby not altering the conduction state of the sample as described above. At higher peak biases, however, hysteresis appears in the *I*−*V* curves. By the time the peak bias is reached, the conductivity state has been changed and the backward curve starts deviating from the forward one. Thus, the FORC-IV loop opening is a method of measuring ionic motion or electrochemical activity, and since *I*−*V* curves were recorded across the grid, samples could be mapped out in terms of the loop opening as shown below. To emphasize the differences between the C-AFM images and FORC-IV maps as well as the differences in the shape of *I*−*V* curves in different locations of the grid, we present *IV*s averaged over the top 10% of the 2500 pixels with highest maximal conductivity (Figure 3(c)) and highest maximal loop opening (Figure 3(d)). As can be seen, highly conductive locations show next to no hysteresis and high current, whereas locations with highest ionic activity manifest huge hysteresis, but at much lower current.

Having described the average behavior, we now turn our attention to local properties of the nanocomposite. Figure 4(a and b) show a C-AFM image of a 500 × 500 nm^2 region taken at 0.1 V and the corresponding topography with a typical high interface conductance, respectively. The FORC-IV loop area maps and current maps at different peak biases are shown in Figure 4 (d,f,h and c,e,g), correspondingly. The loop area maps were normalized to the square of the peak bias divided by 200 MΩ (protective resistance) to render them comparable (units changed from nW to a fraction of unity). At 3 V peak bias (and lower biases that are not shown here), the loop area map is noise-dominated, highlighting areas with high conductivity. However, at 5 and 7 V peak biases, loop area maps clearly show that maximal ionic activity is confined to the interface between BFO and CFO. It is noted that the current maps and loop area maps show slightly different features since the highest conductivity does not correspond to the highest ionic activity, as we have seen in Figure 3(c and d). Activation of switching behavior at different locations with different voltage levels can be seen in the lower left corner of Figure 4(f and h) with a puzzle-piece-like CFO island (encircled in red in Figure 4(c)). At 5 V, its right interface (blue arrow in Figure 4(f)) is active, but by the next sweep at 7 V it already switched to higher conductivity and showed almost the same loop opening as at the island's surface. The rectangular island at the center, on the other hand, got activated more at 7 V, and its interface (green arrow in Figure 4(h)) stands out clearly. Beyond the peak bias of 7 V, the SPM tip starts degrading and the FORC-IV data become less reliable. Thus, in the bias window of 3−7 V, the nanocomposite not only shows higher general ionic activity at the BFO−CFO interface but also differentiates in the switching activation on different interfaces, which further supports that oxygen vacancies play a key role in the modulation of this local conduction.

On the basis of the experimental results, we now focus on the modulation origin of this conduction. In previous studies, oxygen vacancies are mobile positive charges in BFO.[18] The negative tip bias can attract

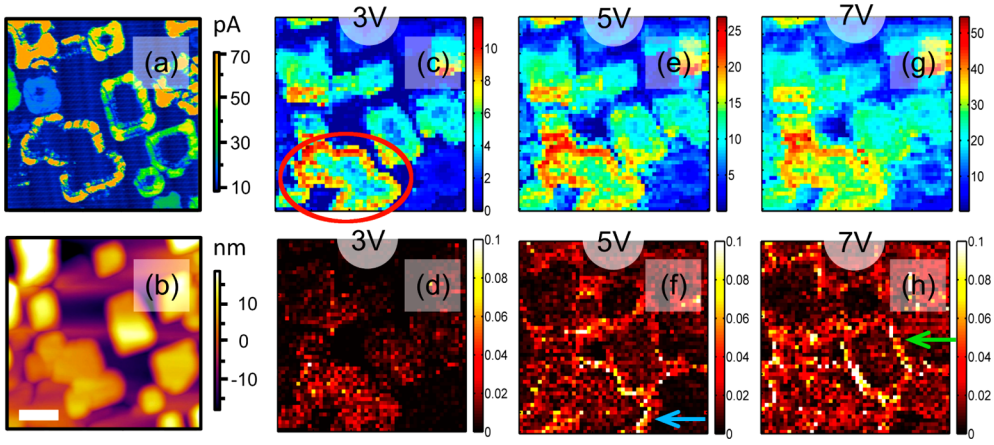

Figure 4. (a) C-AFM image of a selected region taken with 0.1 V applied to the tip and (b) corresponding topography image (scale bar is 100 nm); (c, e, g) current maps at peak biases 3, 5, and 7 V, respectively (scale in nA) plotted from the FORC-IV data collected on a 50 × 50 grid of the same region; (d, f, h) FORC-IV loop area maps showing progressively increasing *I*−*V* hysteresis at the interface.

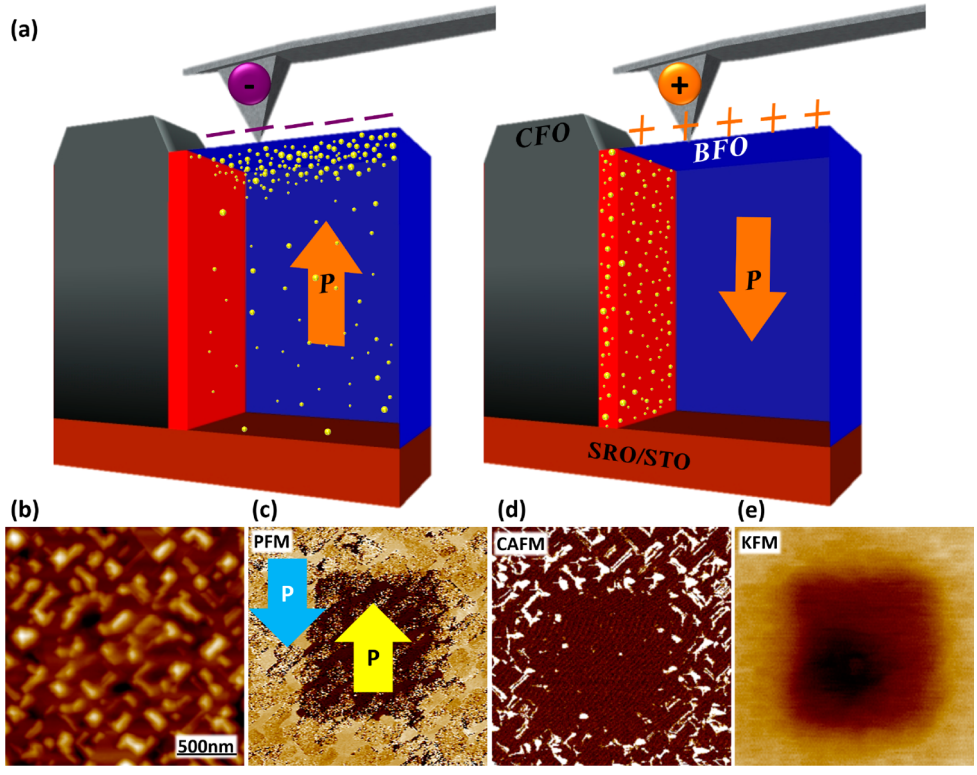

Figure 5. (a) Schematic illustrating the control of the local conduction at the interface. The oxygen vacancies will be attracted by the negative tip bias and thus accumulate on the top surface, making the BFO become a p−n junction. The process is reversible and the interface will be conductive once the positive tip bias is applied. (b) Topography. (c) PFM after switching. Before switching, the PFM shows that the orientation of the out-of-plane phase for the BFO matrix is downward. After switching, the orientation of the out-of-plane phase will be changed to upward. (d) C-AFM image showing that the interface conduction at the area after switching is diminished. (e) KFM image showing the negative surface potential at the poled region.

oxygen vacancies that accumulate on the top surface; consequently, the top surface acquires n-type carriers, whereas the region near the bottom becomes p-type. Therefore, a p−n junction is created in BFO, modifying the conducting behaviors in BFO (typically enhancing the local conduction). We have tested the BFO matrix, and it shows the same characteristics. However, this behavior is opposite our observation in BFO−CFO system (when the positive tip bias was applied, the local conduction can be enhanced). The hypothesis we propose is that due to different polarizabilty of the matrix and the interface, applying a negative tip bias to the interface region would lead to a negatively charged matrix near the interface, and then the positive oxygen vacancies at the interface would be attracted by this electric field to the BFO matrix (Figure 5). In order to

verify this model, PFM, C-AFM, and Kelvin force microscopy (KFM) measurements were carried out (Figure 5). We found that the orientation of out-of-plane polarization is the key to the conduction at the interface and matrix. At the as-grown state, the orientation of out-of-plane polarization is downward, and the interface is conductive. After poling, the orientation of out-of-plane polarization becomes upward, and the conduction at the interface is diminished. The explanation for the phenomenon is that after poling the electrons are trapped at the surface due to the upward polarization. Therefore, the surface potential is negative at the poled area.[19] The negative surface potential of the BFO matrix causes the oxygen vacancies at the interface to move to the top surface of the BFO matrix. In addition, we observe that the BFO matrix poled by a large negative tip bias will need a smaller critical voltage (<2 V) to turn on currents than the as-grown state (Supporting Information). This is because the oxygen vacancies leave from the interface and accumulate on the top surface of the BFO matrix after a negative tip bias is applied, and the BFO matrix is more conductive while the conduction at the interface is degraded. When positive tip bias was applied, the whole process was inversely recovered, and then the interface conduction went back again, suggesting an electrical modulation of the local conduction.

CONCLUSION

In summary, a self-assembled heterointerface delivers a new type of oxide interfaces and provides a huge playground to design new intriguing functionalities. In this study, we have taken the BFO−CFO as a model system to demonstrate a pathway to control the local conduction of this nonvolatile interface. The static and dynamic modulation behaviors were carefully studied by scanning probe microscopy. The mechanism behind this intriguing effect is attributed to the movement of oxygen vacancies; negative bias pumps out the oxygen vacancies and positive bias moves oxygen vacancies back to the interface. Our results suggest the possibility of using this type of oxide device to design next-generation electronic devices.

METHODS

The samples were fabricated by pulsed laser deposition at 700 °C in O_2 (200 mTorr) using a composite target with 65% BFO and 35% CFO (molar ratio).[12] Commercial scanning probe microscope systems (CPII, Multimode 8 with ScanAsyst) were used to perform the measurements of C-AFM, PFM, and KFM. A Pt−Ir-coated tip with a force constant of about 2−4.4 N/m (OSCM-PIT, Olympus) was used for scanning. The voltage pulses for switching the conduction at the interface were performed by an arbitrary waveform generator (G5100A, PICOTEST).

The FORC-IV measurements were performed on a Cypher (Asylum Research) AFM interfaced with National Instrument cards controlled by LabVIEW and Matlab software. Cantilevers with Cr/Pt conductive coating were used (Budget Sensors). Bias was applied to the cantilever tip, and the current was read off the bottom electrode with a Femto current amplifier (DLPCA-200). The voltage waveform had a step height of 0.1 V and a step duration of 20 ms. A protective resistor of 200 MΩ was connected in series with the sample. Data processing was done using custom-written Matlab codes.

Conflict of Interest: The authors declare no competing financial interest.

Acknowledgment. This work was supported by the National Science Council, R.O.C. (NSC-101-2119-M-009-003-MY2), Ministry of Education (MOE-ATU 101W961), and Center for Interdisciplinary Science of National Chiao Tung University. Part of this research was conducted at the Center for Nanophase Materials Sciences, which is sponsored at Oak Ridge National Laboratory by the Scientific User Facilities Division, Office of Basic Energy Sciences, U.S. Department of Energy.

Supporting Information Available: Additional data and text are described. This material is available free of charge *via* the Internet at http://pubs.acs.org.

REFERENCES AND NOTES

1. Hwang, H. Y.; Iwasa, Y.; Kawasaki, M.; Keimer, B.; Nagaosa, N.; Tokura, Y. Emergent Phenomena at Oxide Interfaces. *Nat. Mater.* **2012**, *11*, 103–113.
2. Takagi, H.; Hwang, H. Y. An Emergent Change of Phase for Electronics. *Science* **2010**, *327*, 1601–1602.
3. Hsieh, Y. H.; Liou, J. M.; Huang, B. C.; Liang, C. W.; He, Q.; Zhan, Q.; Chiu, Y. P.; Chen, Y. C.; Chu, Y. H. Local Conduction at the $BiFeO_3$-$CoFe_2O_4$ Tubular Oxide Interface. *Adv. Mater.* **2012**, *24*, 4564–4568.
4. Ohtomo, A.; Hwang, H. Y. A High-Mobility Electron Gas at the $LaAlO_3$/$SrTiO_3$ Heterointerface. *Nature* **2004**, *427*, 423–426.
5. Chu, Y. H.; He, Q.; Yang, C. H.; Yu, P.; Martin, L. W.; Shafer, P.; Ramesh, R. Nanoscale Control of Domain Architectures in $BiFeO_3$ Thin Films. *Nano Lett.* **2009**, *9*, 1726–1730.
6. Seidel, J.; Martin, L. W.; He, Q.; Zhan, Q.; Chu, Y. H.; Rother, A.; Hawkridge, M. E.; Maksymovych, P.; Yu, P.; Gajek, M.; *et al*. Conduction at Domain Walls in Oxide Multiferroics. *Nat. Mater.* **2009**, *8*, 229–234.
7. Guyonnet, J.; Gaponenko, I.; Gariglio, S.; Paruch, P. Conduction at Domain Walls in Insulating $Pb(Zr_{0.2}Ti_{0.8})O_3$ Thin Films. *Adv. Mater.* **2011**, *23*, 5377–5382.
8. Wu, W.; Horibe, Y.; Lee, N.; Cheong, S.-W.; Guest, J. R. Conduction of Topologically Protected Charged Ferroelectric Domain Walls. *Phys. Rev. Lett.* **2012**, *108*, 077203.
9. Meier, D.; Seidel, J.; Cano, A.; Delaney, K.; Kumagai, Y.; Mostovoy, M.; Spaldin, N. A.; Ramesh, R.; Fiebig, M. Anisotropic Conductance at Improper Ferroelectric Domain Walls. *Nat. Mater.* **2012**, *11*, 284–288.
10. Maksymovych, P.; Seidel, J.; Chu, Y. H.; Wu, P. P.; Baddorf, A. P.; Chen, L. Q.; Kalinin, S. V.; Ramesh, R. Dynamic Conductivity of Ferroelectric Domain Walls in $BiFeO_3$. *Nano Lett.* **2011**, *11*, 1906–1912.
11. Thiel, S.; Hammerl, G.; Schmehl, A.; Schneider, C. W.; Mannhart, J. Tunable Quasi-Two-Dimensional Electron Gases in Oxide Heterostructures. *Science* **2006**, *313*, 1942–1945.
12. Liao, S. C.; Tsai, P. Y.; Liang, C. W.; Liu, H. J.; Yang, J. C.; Lin, S. J.; Lai, C. H.; Chu, Y. H. Misorientation Control and Functionality Design of Nanopillars in Self-Assembled Perovskite-Spinel Heteroepitaxial Nanostructures. *ACS Nano* **2011**, *5*, 4118–4122.
13. Zheng, H. M.; Straub, F.; Zhan, Q.; Yang, P. L.; Hsieh, W. K.; Zavaliche, F.; Chu, Y. H.; Dahmen, U.; Ramesh, R. Self-assembled Growth of $BiFeO_3$-$CoFe_2O_4$ Nanostructures. *Adv. Mater.* **2006**, *18*, 2747–2752.

14. Zhan, Q.; Yu, R.; Crane, S. P.; Zheng, H.; Kisielowski, C.; Ramesh, R. Structure and Interface Chemistry of Perovskite-Spinel Nanocomposite Thin Films. *Appl. Phys. Lett.* **2006**, *89*, 172902.
15. Balke, N.; Winchester, B.; Ren, W.; Chu, Y. H.; Morozovska, A. N.; Eliseev, E. A.; Huijben, M.; Vasudevan, R. K.; Maksymovych, P.; Britson, J.; *et al*. Enhanced Electric Conductivity at Ferroelectric Vortex Cores in $BiFeO_3$. *Nat. Phys.* **2012**, *8*, 81–88.
16. Seidel, J.; Maksymovych, P.; Batra, Y.; Katan, A.; Yang, S. Y.; He, Q.; Baddorf, A. P.; Kalinin, S. V.; Yang, C. H.; Yang, J. C.; *et al*. Domain Wall Conductivity in La-Doped $BiFeO_3$. *Phys. Rev. Lett.* **2010**, *105*, 197603.
17. Strelcov, E.; Kim, Y.; Jesse, S.; Wang, C. H.; Teng, Y. C.; Chu, Y. H.; Kalinin, S. V. Probing Local Ionic Dynamics in Functional Oxides at the Nanoscale. *Nano Lett.* **2013**, *13*, 3455–3462.
18. Yang, C. H.; Seidel, J.; Kim, S. Y.; Rossen, P. B.; Yu, P.; Gajek, M.; Chu, Y. H.; Martin, L. W.; Holcomb, M. B.; He, Q.; *et al*. Electric Modulation of Conduction in Multiferroic Ca-Doped $BiFeO_3$ Films. *Nat. Mater.* **2009**, *8*, 485–493.
19. Chen, Y. C.; Ko, C. H.; Huang, Y. C.; Yang, J. C.; Chu, Y. H. Domain Relaxation Dynamics in Epitaxial $BiFeO_3$ Films: Role of Surface Charges. *J. Appl. Phys.* **2012**, *112*, 052017.